nature neuroscience

Social learning and amygdala disruptions in Nf1 mice are rescued by blocking p21-activated kinase

Andrei I Molosh[1,2,11], Philip L Johnson[1–3,11], John P Spence[1,4], David Arendt[1], Lauren M Federici[2–4], Cristian Bernabe[3], Steven P Janasik[1], Zaneer M Segu[5], Rajesh Khanna[2,6], Chirayu Goswami[7], Weiguo Zhu[2,6], Su-Jung Park[8], Lang Li[7], Yehia S Mechref[5], D Wade Clapp[8,9] & Anantha Shekhar[1,2,6,10]

Children with neurofibromatosis type 1 (NF1) are increasingly recognized as having a high prevalence of social difficulties and autism spectrum disorders (ASDs). We demonstrated a selective social learning deficit in mice with deletion of a single *Nf1* allele (*Nf1*$^{+/-}$), along with greater activation of the mitogen-activated protein kinase pathway in neurons from the amygdala and frontal cortex, structures that are relevant to social behaviors. The *Nf1*$^{+/-}$ mice showed aberrant amygdala glutamate and GABA neurotransmission, deficits in long-term potentiation and specific disruptions in the expression of two proteins that are associated with glutamate and GABA neurotransmission: a disintegrin and metalloprotease domain 22 (Adam22) and heat shock protein 70 (Hsp70), respectively. All of these amygdala disruptions were normalized by the additional deletion of the p21 protein-activated kinase (Pak1) gene. We also rescued the social behavior deficits in *Nf1*$^{+/-}$ mice with pharmacological blockade of Pak1 directly in the amygdala. These findings provide insights and therapeutic targets for patients with NF1 and ASDs.

Affecting roughly 1 in 3,000 children worldwide, NF1 is one of the most common single-gene disorders, resulting in the development of complex tumors known as neurofibromas and marked cognitive and learning disabilities[1,2]. A number of studies have demonstrated deficits in social information processing and social behaviors in over 50% of patients with NF1 (refs. 3–6), with 20–30% of patients reaching the severity of clinical diagnosis of ASD[7–9]. Further analyses of these social deficits in patients with NF1 suggested that they also have problems in facial emotional recognition (especially fear), a task that is linked specifically to human amygdala function[6,10].

Thus, NF1 mutation presents an important single-gene disruption model that could provide insights into the molecular mechanisms for social learning deficits and the pathophysiology of ASDs. Social learning is the product of complex interactions between multiple structures in the CNS, particularly the amygdala, striatum, hippocampus, fusiform area and frontal cortex[11–13]. Using homologous recombination to disrupt the mouse homolog of *NF1* (*Nf1*), we found that loss of a single *Nf1* allele in mice (*Nf1*$^{+/-}$ mice) reduced neurofibromin levels in multiple organs, recapitulating the phenotypes of the human condition[14]. Specifically, this alteration caused deficits in some forms of spatial learning, as well as disrupted hippocampal long-term potentiation (LTP)[15,16]. In addition to effects in the hippocampus, *Nf1*$^{+/-}$ mice also showed similar reductions in neurofibromin levels in the amygdala and frontal cortex, CNS sites that are critical for social behaviors and emotional regulation. Therefore, we conducted the present study to test whether *Nf1*$^{+/-}$ mice demonstrate disruptions in social behaviors and elucidate the cellular or molecular changes in CNS sites that are associated with social behaviors.

RESULTS

Nf1$^{+/-}$ mice show social learning deficits and hyperactivation of Mapk in the brain

To determine whether *Nf1*$^{+/-}$ mice demonstrate disrupted social learning, we used a well-validated three-chamber social memory test[17]. On initial exposure to the testing apparatus, both wild-type (WT) and *Nf1*$^{+/-}$ mice spent significantly more time interacting with an unfamiliar mouse over an inanimate object (n = 12, 12 (WT, *Nf1*$^{+/-}$); side-preference effect $F_{1,22} = 105.8$, $P < 0.001$, but no *Nf1*$^{+/-}$ interaction $F_{1,22} = 0.9$, $P = 0.358$; **Fig. 1a**), demonstrating that the *Nf1*$^{+/-}$ genotype does not affect conspecific social cue recognition in mice (we labeled this as the baseline social behavior). After a 10-min interval, we retested the mice with a choice between a novel mouse and the previous familiar mouse to assess their short-term social memory[18]. Mice from both the WT and *Nf1*$^{+/-}$ genotypes spent significantly more time with the new mouse (n = 12, 12; side preference effect $F_{1,22} = 105.8$, $P < 0.001$, but no *Nf1*$^{+/-}$ interaction $F_{1,22} = 0.4$, $P = 0.554$; **Fig. 1b**), suggesting that *Nf1*$^{+/-}$ mice show a normal ability to discriminate and immediately recall social cues. However, when presented

[1]Department of Psychiatry, Institute of Psychiatric Research, Indiana University School of Medicine, Indianapolis, Indiana, USA. [2]Stark Neurosciences Research Institute, Indiana University School of Medicine, Indianapolis, Indiana, USA. [3]Department of Anatomy and Cell Biology, Indiana University School of Medicine, Indianapolis, Indiana, USA. [4]Program in Medical Neurosciences, Indiana University School of Medicine, Indianapolis, Indiana, USA. [5]Department of Chemistry, METACyt Biochemical Analysis Center, Indiana University, Bloomington, Indiana, USA. [6]Department of Pharmacology and Toxicology, Indiana University School of Medicine, Indianapolis, Indiana, USA. [7]Center for Computational Biology and Bioinformatics, Indiana University School of Medicine, Indianapolis, Indiana, USA. [8]Wells Center for Pediatric Research, Department of Pediatrics, Indiana University School of Medicine, Indianapolis, Indiana, USA. [9]Department of Microbiology and Immunology, Indiana University School of Medicine, Indianapolis, Indiana, USA. [10]Indiana Clinical and Translational Sciences Institute, Indiana University School of Medicine, Indianapolis, Indiana, USA. [11]These authors contributed equally to this work. Correspondence should be addressed to A.S. (ashekhar@iu.edu).

Received 14 June; accepted 26 August; published online 21 September 2014; doi:10.1038/nn.3822

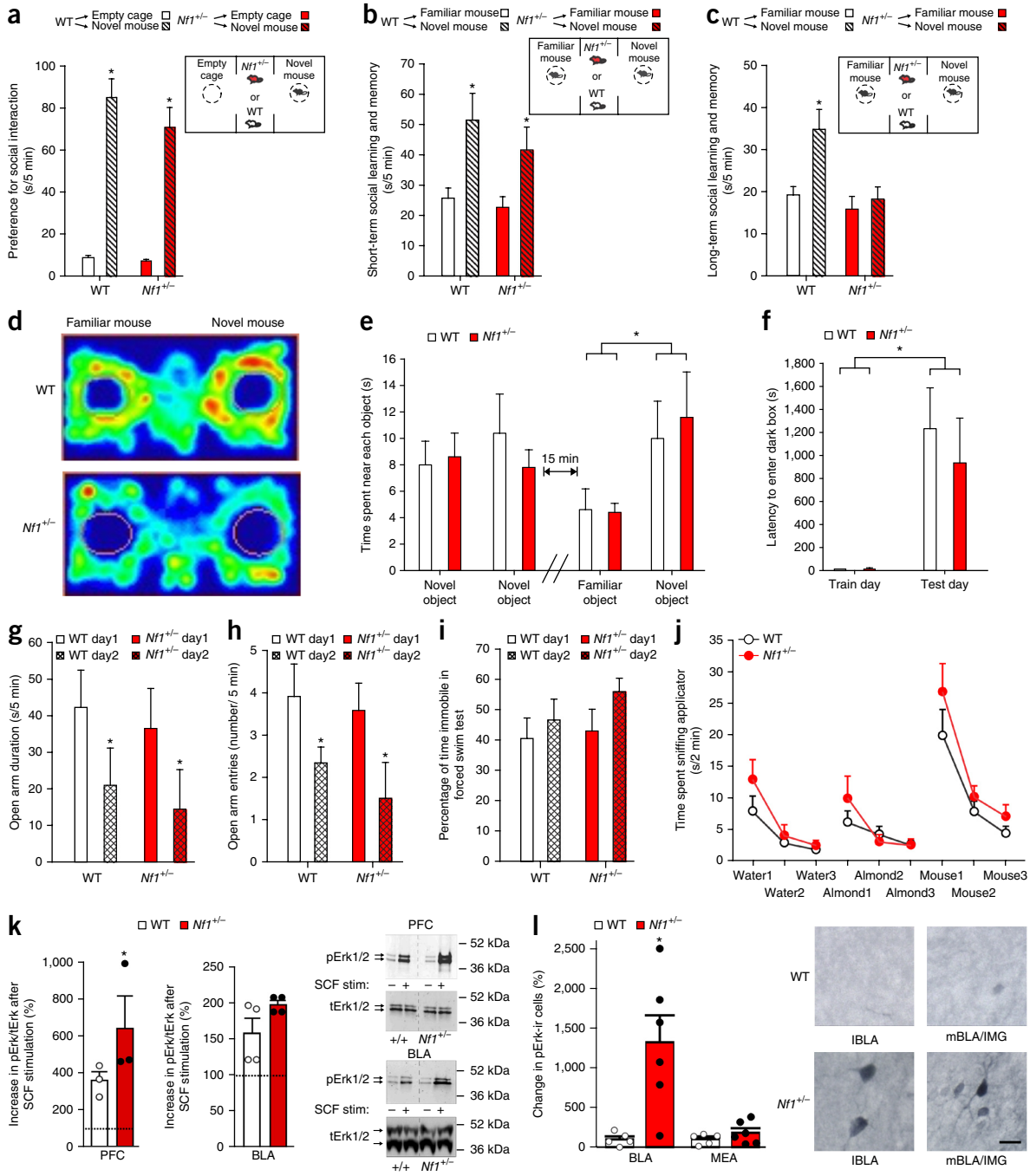

Figure 1 *Nf1*$^{+/-}$ mice show selective deficits in long-term social learning and increased Mapk activation in the amygdala. (**a**–**c**) Time spent sniffing wire cages containing 'stimulus' mice in a three-chambered apparatus (insets illustrate the orientation of the cages and when cages were empty or contained a novel or familiar mouse). (**a**) WT and *Nf1*$^{+/-}$ mouse preferences for social interaction. * indicates only a side preference effect ($P < 0.001$). (**b**) Short-term social learning (1–3 min after exposure to the 'test' mouse). * indicates only a side preference effect ($P < 0.001$). (**c**) Long-term social learning, as measured by preference for social novelty (24 h after exposure to the test mouse). * indicates a side preference effect ($P = 0.005$) and a *Nf1*$^{+/-}$ interaction ($P = 0.032$). (**d**) Heat maps of the time spent in each region for the long-term social learning test. (**e**,**f**) Learning in the novel object recognition test (* indicates only an object preference, $P = 0.017$) (**e**) and passive avoidance test (* indicates only an object preference, $P = 0.001$) (**f**). (**g**,**h**) Anxiety states in the elevated plus maze. * indicates only a time effect (both $P = 0.003$). (**i**) Depression or despair in the forced swim test. (**j**) Olfaction in an olfactory habituation test. (**k**) Left, genotype association with Mapk hyperexcitation in neuronal cultures from the prefrontal cortex (PFC). *$P = 0.017$. Middle, Mapk hyperexcitation in the BLA region of *Nf1*$^{+/-}$ and WT mice. Right, representative cropped western blot gels from the bar graph data illustrating pErk1/2 in cultured cortical neurons at basal levels and 2 min after stimulation with SCF (10 ng/ml); total Erk1/2 was used as a loading control (full-length blots and gels are presented in **Supplementary Fig. 3**). (**l**) Left, Mapk hyperexcitation in cells immunoreactive for pErk (pErk-ir) within the BLA and medial amygdala (MEA) of *Nf1*$^{+/-}$ mice exposed to a novel mouse. *$P = 0.010$. Right, high-magnification photographs showing pErk-immunoreactive cells in the lateral BLA (lBLA) and medial BLA and amygdaloid intermedullary gray (mBLA/IMG) of WT and *Nf1*$^{+/-}$ mice. Scale bar, 15 μm. All graphs depict the mean ± s.e.m. for WT (white) and *Nf1*$^{+/-}$ (red) mice. Statistical analyses in **a**–**c** were performed by one-way analysis of variance (ANOVA) with genotype as the main factor and side preference as a repeated measure.

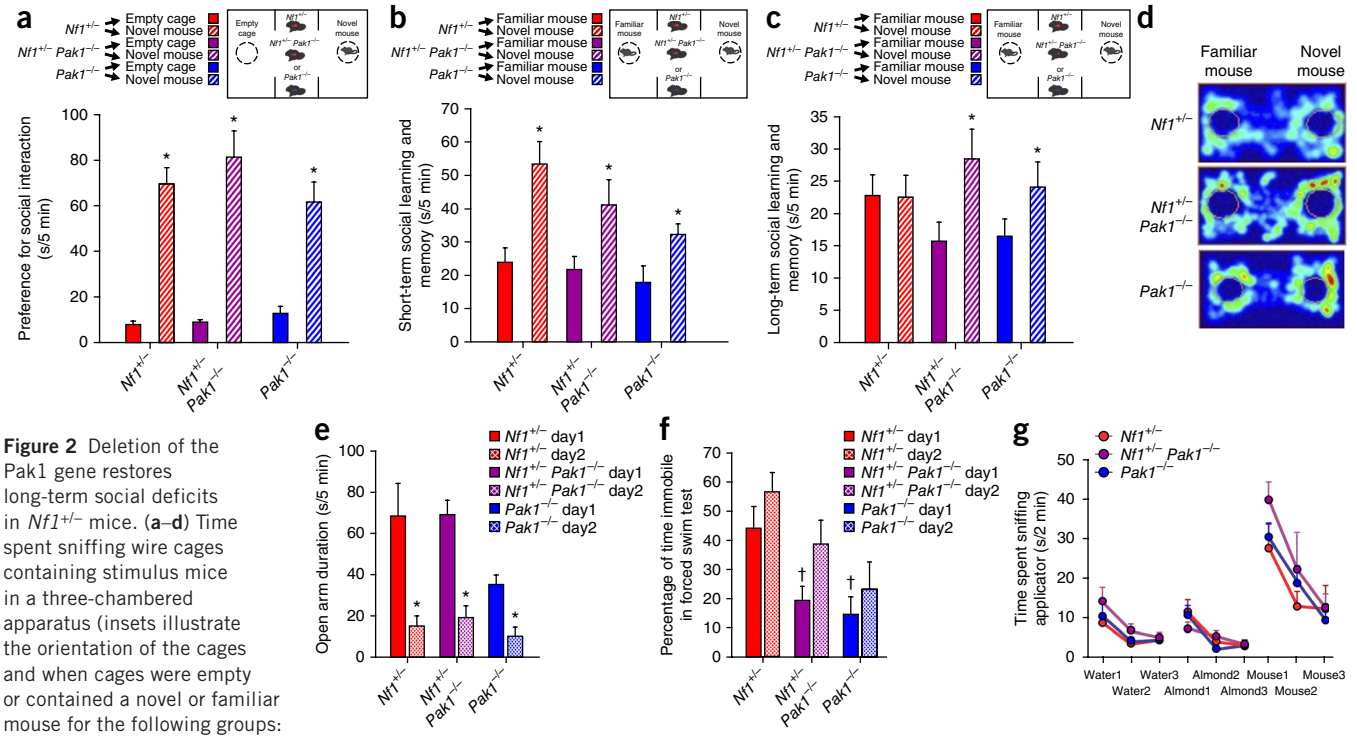

Figure 2 Deletion of the Pak1 gene restores long-term social deficits in *Nf1*$^{+/-}$ mice. (**a**–**d**) Time spent sniffing wire cages containing stimulus mice in a three-chambered apparatus (insets illustrate the orientation of the cages and when cages were empty or contained a novel or familiar mouse for the following groups: *Nf1*$^{+/-}$, *Nf1*$^{+/-}$ *Pak1*$^{-/-}$ and *Pak1*$^{-/-}$). (**a**) Preference for social interaction. * indicates only a side preference effect ($P < 0.001$). (**b**) Short-term social learning. * indicates only a side preference effect ($P < 0.001$). (**c**) Preference for social novelty and long-term social learning (24 h after exposure to the test mouse). * indicates a Fisher's exact test determining that *Nf1*$^{+/-}$ *Pak1*$^{-/-}$ mice showed a greater novel mouse preference (≥10 s criteria) than *Nf1*$^{+/-}$ mice, $P = 0.036$ and a genotype × side preference interaction that approached significance, $P = 0.054$. (**d**) Comprehensive heat maps of time spent in each region in the long-term social learning test. (**e**) Anxiety as measured by elevated plus maze. * indicates only a time effect ($P < 0.001$). (**f**) Depression-associated behavior. † indicates a genotype effect on day 1 ($P = 0.004$). (**g**) Olfactory habituation. All graphs depict the mean ± s.e.m. for *Nf1*$^{+/-}$ (red), *Nf1*$^{+/-}$ *Pak1*$^{-/-}$ (purple) and *Pak1*$^{-/-}$ (blue) mice. The statistical analyses in **a**–**c** were performed by one-way ANOVA with genotype as the main factor and side preference as a repeated measure.

with yet another novel mouse and the previously familiar mouse 24 h later, the *Nf1*$^{+/-}$ mice did not show increased exploration of the novel mouse compared to the familiar mouse, whereas the WT mice showed robust preference for the novel mouse ($n = 12, 11$; side preference effect $F_{1,21} = 9.9$, $P = 0.005$, and an *Nf1*$^{+/-}$ interaction $F_{1,21} = 5.3$, $P = 0.032$; **Fig. 1c**,**d**). These results indicate that *Nf1*$^{+/-}$ mice, although showing normal immediate social discrimination at baseline, were unable to retain or recall the social memory and discriminate between familiar and unfamiliar social cues after a 24-h delay.

To determine whether this deficit was selective for social learning or was generalized to other amygdala-cortical circuits, we also tested the performance of *Nf1*$^{+/-}$ mice in other novelty and emotional learning paradigms. We confirmed that compared to WT mice, *Nf1*$^{+/-}$ mice did not demonstrate deficits in learning in a novel object recognition test ($n = 5, 5$; object preference effect $F_{1,8} = 8.9$, $P = 0.017$, but no *Nf1*$^{+/-}$ interaction; **Fig. 1e**) or in avoidance learning in a passive avoidance test ($n = 9, 6$; avoidance effect $F_{1,13} = 16.1$, $P = 0.001$, but no *Nf1*$^{+/-}$ interaction; **Fig. 1f**). We also tested the ability of the mice to demonstrate innate avoidance 24 hours after exposure to a fear stimulus by using the elevated plus maze, as described previously[19]. When we tested mice 24 h later, both genotypes showed similar increases in the avoidance of the open arms, suggesting normal retention of memory for aversive cues and avoidance in both genotypes ($n = 12, 12$; a day effect for duration $F_{1,22} = 10.1$, $P = 0.003$ and entries $F_{1,22} = 11.5$, $P = 0.003$ in the open arms, but no *Nf1*$^{+/-}$ interactions; **Fig. 1g**,**h**). Similarly, using the Porsolt forced swim test, we measured the development of behavioral despair 24 h after the swim stress test in the *Nf1*$^{+/-}$ mice. The WT and *Nf1*$^{+/-}$ mice both showed normal learning in the forced swim test ($n = 12, 12$; day effect $F_{1,22} = 5.1$, $P = 0.034$, but no *Nf1*$^{+/-}$ interaction; **Fig. 1i**). We also tested the *Nf1*$^{+/-}$ mice for differences in ability to discriminate olfactory cues, another possible confounder that could result in mice showing poor social learning. In a standardized olfactory habituation test, both WT and *Nf1*$^{+/-}$ mice demonstrated similar learning ($n = 6, 6$; water: test effect $F_{2,20} = 15.2$, $P < 0.001$; almond: test effect $F_{2,20} = 7.4$, $P = 0.004$; novel mouse: test effect $F_{2,20} = 37.1$, $P < 0.001$; no *Nf1*$^{+/-}$ interactions; **Fig. 1j**). Thus, *Nf1*$^{+/-}$ mice appeared to have selective and circumscribed deficits in long-term retention of social information.

The *NF1* gene encodes neurofibromin, which negatively regulates Ras GTPase activation (a hypothetical illustration is shown in **Supplementary Fig. 1a**). Mutation at the *Nf1* locus increases the output of Mapk and Pi3k signal transduction from the cellular membrane to the nucleus, resulting in the hyperactivation of the products of its downstream pathways, such as phosphorylated Erk (pErk)[20,21]. Therefore, we first tested whether neurons cultured from *Nf1*$^{+/-}$ mice displayed a similar hyperactivation of Mapk after growth factor stimulation. Application of recombinant murine stem cell factor (SCF; 10 ng/ml) increased the levels of pErk1 and pErk2 (pErk1/2) to a significantly greater degree in frontal cortical neurons cultured from *Nf1*$^{+/-}$ mice when compared to those cultured from WT mice ($n = 3, 3$; pErk compared to total Erk (tErk) after stimulation, $t_4 = -4.0$, $P = 0.017$; **Fig. 1k**). Applying SCF to amygdala cultures from *Nf1*$^{+/-}$ mice increased pErk1/2 by ~100%, compared to a ~50% increase observed in cultures from WT mice ($n = 4, 4$; pErk to tErk after stimulation, $t_6 = -1.8$, $P = 0.114$; **Fig. 1k**). To complement these *in vitro* findings, we also assessed pErk immunostaining in subregions

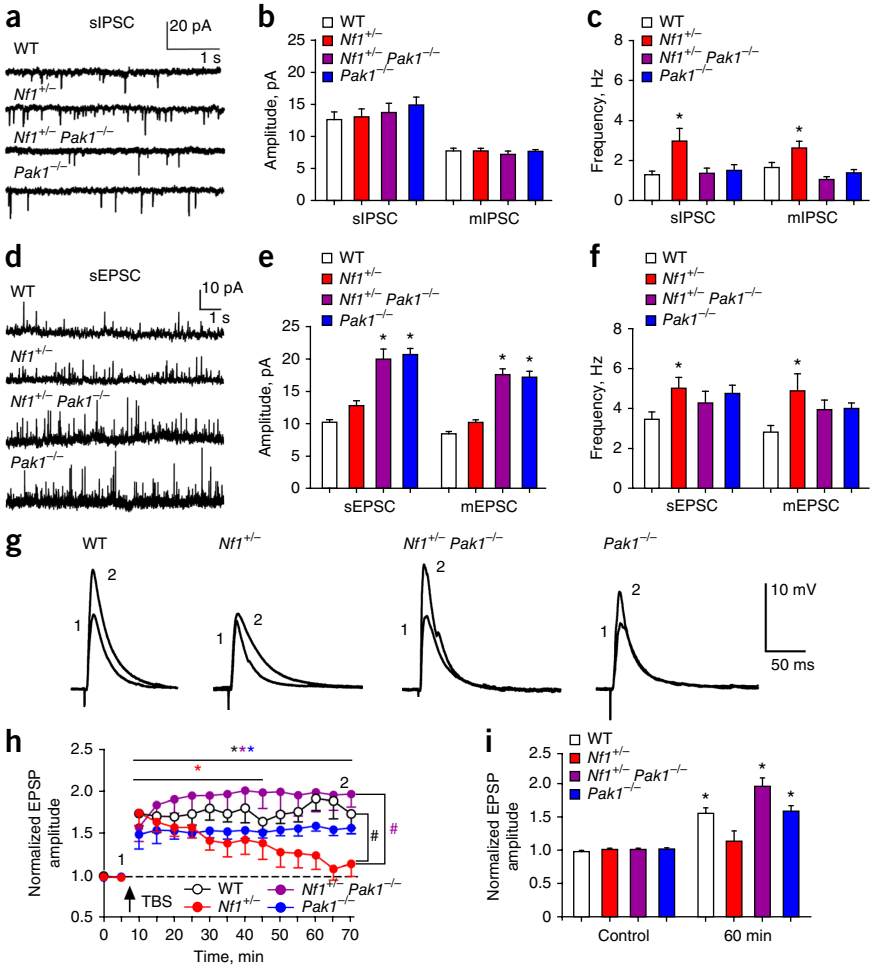

Figure 3 *Nf1*$^{+/-}$ mice have elevated GABA-glutamate neurotransmission and disrupted LTP in the amygdala, which was restored by deletion of *Pak1*. (**a**) Representative electrophysiological recordings of sIPSCs at a holding potential of –55 mV from pyramidal neurons of the BLA of WT (n = 11 cells), *Nf1*$^{+/-}$ (n = 11 cells), *Nf1*$^{+/-}$ *Pak1*$^{-/-}$ (n = 14 cells) and *Pak1*$^{-/-}$ (n = 14 cells) mice. (**b**,**c**) sIPSC and mIPSC amplitude (**b**) and frequency (**c**) in the BLA of mice from the groups indicated (n = 11, 11, 14, 14 cells for the groups listed top to bottom in the legend). *P = 0.017 (sIPSCs) and *P = 0.004 (mIPSCs) compared to WT. (**d**) Representative recordings of isolated sEPSCs and mEPSCs from BLA pyramidal neurons at a holding potential of –60 mV in WT (n = 17 cells), *Nf1*$^{+/-}$ (n = 14 cells), *Nf1*$^{+/-}$ *Pak1*$^{-/-}$ (n = 16 cells) and *Pak1*$^{-/-}$ (n = 19 cells) mice. (**e**,**f**) Amplitude (**e**) and frequency (**f**) of sEPSCs (n = 17, 14, 16, 19 cells) and mEPSCs (n = 17, 15, 13, 15 cells). *P = 0.037 (sEPSCs) and *P = 0.05 (mEPSCs) compared to WT. (**g**) Representative traces of EPSPs before (1) and 60 min after (2) TBS stimulation of thalamic inputs to the BLA at a holding potential of –70 mV from pyramidal neurons of the BLA of WT (n = 7 cells), *Nf1*$^{+/-}$ (n = 12 cells), *Nf1*$^{+/-}$ *Pak1*$^{-/-}$ (n = 8 cells) and *Pak1*$^{-/-}$ (n = 5 cells) mice. (**h**) Time course of averaged evoked EPSCs in response to TBS stimulation of thalamic afferents in all neurons recorded from WT (white circle), *Nf1*$^{+/-}$ (red), *Nf1*$^{+/-}$ *Pak1*$^{-/-}$ (purple) and *Pak1*$^{-/-}$ (blue) mice. * and # indicate a *Nf1*$^{+/-}$ × *Pak1*$^{-/-}$ × time interaction, $P < 0.0001$, with * and # indicating over-time effects and genotype effects, respectively, at each time point. (**i**) Summary graph showing group data for the effects of the tetanic stimulation protocol on EPSP amplitude before (control) and 60 min after stimulation in WT (white, n = 7 cells), *Nf1*$^{+/-}$ (red, n = 12 cells), *Nf1*$^{+/-}$ *Pak1*$^{-/-}$ (purple, n = 8 cells) and *Pak1*$^{-/-}$ (blue, n = 5 cells) mice. All graphs depict the mean ± s.e.m. for each group. Statistical analyses in **b**, **c**, **e**, **f** and **i** were performed by two-way ANOVA with genotypes as the main factors. Statistical analyses in **h** were performed by two-way ANOVA with genotypes as the main factors and time as a repeated measure.

of the amygdala in WT and *Nf1*$^{+/-}$ mice after exposure to a novel mouse. Compared to WT mice, *Nf1*$^{+/-}$ mice had increased numbers of pErk-immunoreactive cells in the basolateral amygdala (BLA; t_9 = 3.2, P = 0.010) but not the medial amygdala (n = 5, 6; t_9 = 1.2, P = 0.262; **Fig. 1l**), further demonstrating the hyperactivity of MAPK pathways in neurons responding to a social cue.

Deletion of *Pak1* restores long-term social deficits in *Nf1*$^{+/-}$ mice

PAK1 is a downstream effector that is regulated by the Rho family of GTPases and positively regulates MAPK activation, and deletion of the Pak1 gene in mice (*Pak1*$^{-/-}$) could potentially normalize the hyperactivation of Mapk pathways seen in *Nf1*$^{+/-}$ mice, as has been demonstrated previously in macrophages[22] (**Supplementary Fig. 1a**). To confirm that this approach could normalize social learning deficits in *Nf1*$^{+/-}$ mice, we tested whether genetic intercross (*Nf1*$^{+/-}$ *Pak1*$^{-/-}$) would restore the learning deficits seen in *Nf1*$^{+/-}$ mice. We found that the *Nf1*$^{+/-}$, *Nf1*$^{+/-}$ *Pak1*$^{-/-}$ and *Pak1*$^{-/-}$ strains showed no differences in baseline social preference (n = 12, 11, 6; side preference effect $F_{1,26}$ = 100.5, P < 0.001, but no genotype interaction; **Fig. 2a**) or short-term social learning (n = 12, 11, 6; side preference effect $F_{1,26}$ = 32.7, P < 0.001, but no genotype interaction; **Fig. 2b**). As in the analyses described above, we observed deficits in *Nf1*$^{+/-}$ mice in long-term social learning, but notably, deletion of *Pak1*$^{-/-}$ in *Nf1*$^{+/-}$ mice (*Nf1*$^{+/-}$ *Pak1*$^{-/-}$) clearly restored this learning deficit (n = 12, 11, 6; side preference effect $F_{1,26}$ = 7.5, P = 0.011, and a genotype × side preference interaction that approached significance $F_{1,26}$ = 3.3, P = 0.054; a Fisher's exact test determined that *Nf1*$^{+/-}$ *Pak1*$^{-/-}$ mice showed a greater novel mouse preference (≥10 s criteria) than *Nf1*$^{+/-}$ mice, P = 0.036; **Fig. 2c**,**d**). Similar to our previous results with *Nf1*$^{+/-}$

Table 1 Protein expression differences in the BLA of *Nf1*$^{+/-}$ mice after deletion of *Pak1*

Protein	Locus ID	Fold change	Description
Cap1[a,b]	P40124	3.05	Adenylate cyclase-associated protein 1
Hsp70[a,b]	P63017	1.71	Heat shock protein 70
Adam22[a,b]	Q9R1V6	–6.17	ADAM metallopeptidase domain 22

Shown are protein expression differences from a total of 380 proteins screened in the BLA of *Nf1*$^{+/-}$ mice that were rescued by deletion of *Pak1* (the corresponding bar graphs are shown in **Fig. 4a**–**c**). Of the 380 proteins that were assessed in the BLA, there were an additional 70 that had significant expression differences in *Nf1*$^{+/-}$ mice compared to WT controls but were not rescued by deletion of *Pak1* (**Supplementary Table 1**). Cap1, *Nf1*$^{+/-}$ × *Pak1*$^{-/-}$ interaction, P = 0.005; Hsp70, *Nf1*$^{+/-}$ × *Pak1*$^{-/-}$ interaction, P = 0.025; Adam22, *Nf1*$^{+/-}$ effect, P < 0.001, and *Pak1*$^{-/-}$ effect, P = 0.048.
[a]Significance with a two-way ANOVA (performed on log-transformed protein expression data).
[b]Significance with ProteinQuant (performed on log-transformed protein expression data).

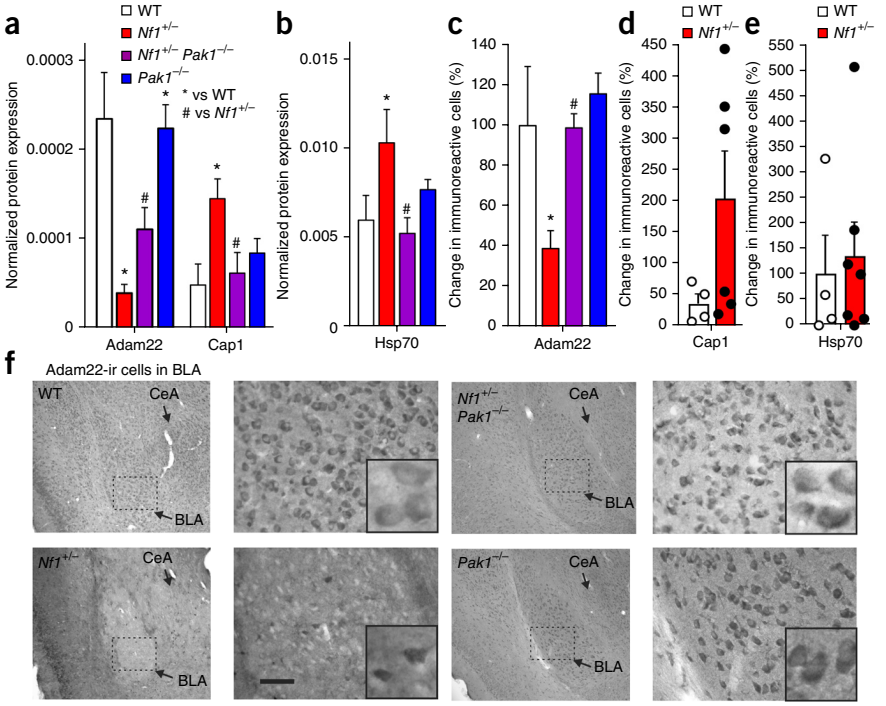

Figure 4 *Nf1*$^{+/-}$ mice have altered Adam22, Cap1 and Hsp70 protein expression levels in the amygdala that are partially rescued by deletion of *Pak1*. (**a**,**b**) Globally normalized protein expression of Adam22 (* and # indicate an *Nf1*$^{+/-}$ effect, $P < 0.001$) and Cap1 (* and # indicate an *Nf1*$^{+/-}$ effect, $P = 0.013$) (**a**) and Hsp70 (* and # indicate an *Nf1*$^{+/-}$ effect, $P = 0.014$; **b**) in the BLA of WT, *Nf1*$^{+/-}$, *Nf1*$^{+/-}$ *Pak1*$^{-/-}$ and *Pak1*$^{-/-}$ mice. Error bars represent the s.e.m. (**c**–**e**) The number of Adam22-immunoreactive (* and # indicate a *Nf1*$^{+/-}$ effect, $P = 0.015$, and a *Pak1*$^{-/-}$ effect, $P = 0.018$) (**c**), Cap1-immunoreactive (**d**) and Hsp70-immunoreactive (**e**) cells in the BLA of WT and *Nf1*$^{+/-}$ mice (as well as in *Nf1*$^{+/-}$ *Pak1*$^{-/-}$ and *Pak1*$^{-/-}$ mice for Adam22). Bars represent the mean, and error bars represent the s.e.m. (**f**) Low-magnification (left) and high-magnification (right) photomicrographs of Adam22-immunoreactive cells in the amygdala of WT, *Nf1*$^{+/-}$, *Nf1*$^{+/-}$ *Pak1*$^{-/-}$ and *Pak1*$^{-/-}$ mice. The central amygdala (CeA) and BLA are indicated with arrows. The dashed-line boxes indicate where cells were counted, as well as the area enlarged in the high-magnification photomicrographs to the right. The scale bar shown indicates 25 μm in the images containing dashed-line boxes, 75 μm in the larger images to their right and 375 μm in the insets. **Supplementary Figure 1b** shows a hypothetical illustration depicting glutamate and GABA regulation of normal EPSC, LTP and IPSC activity in WT mice and how disruption of Adam22 in *Nf1*$^{+/-}$ mice interrupts anchoring of AMPA receptors to the postsynaptic membrane and leads to nonsustainable LTP (as demonstrated in **Fig. 3h**). Similarly, increased expression of Hsp70 could contribute to increases in presynaptic GABA release and an increased frequency of IPSCs (seen in **Fig. 3c**). Statistical analyses in **a**–**c** were performed by two-way ANOVA with genotypes as the main factors, and those in **d** and **e** were performed by unpaired two-tailed *t* test.

mice, we detected no differences in anxiety ($n = 12, 11, 6$; day effect $F_{2,26} = 36.6$, $P < 0.001$, but no genotype interaction; **Fig. 2e**) or olfaction ($n = 12, 11, 6$; test 1–3 effects were noted for water $F_{2,30} = 12.2$, $P < 0.001$, almond $F_{2,30} = 23.2$, $P < 0.001$ and novel mouse $F_{2,30} = 26.3$, $P < 0.001$, but not genotype interactions; **Fig. 2g**) between the *Nf1*$^{+/-}$ and *Nf1*$^{+/-}$ *Pak1*$^{-/-}$ mice. Although despair-associated behaviors were not different between WT and *Nf1*$^{+/-}$ mice (**Fig. 1i**), compared to *Nf1*$^{+/-}$ mice, the *Nf1*$^{+/-}$ *Pak1*$^{-/-}$ and *Pak1*$^{-/-}$ mice had reduced despair-associated immobility ($n = 12, 11, 6$; genotype effect $F_{2,26} = 6.9$, $P = 0.004$ and day effect $F_{2,26} = 9.2$, $P = 0.005$, but no genotype interaction; **Fig. 2f**). Overall, these results show that constitutive *Pak1* deletion could rescue the social learning deficits in *Nf1*$^{+/-}$ mice.

Deletion of *Pak1* rescues disrupted amygdala network and LTP in *Nf1*$^{+/-}$ mice

Because the amygdala is important in social learning[11–13] and we observed hyperactivity of Mapk pathways in BLA neurons of *Nf1*$^{+/-}$ mice after novel mouse exposure (**Fig. 1l**), we next assessed functional changes in the amygdala networks in WT, *Nf1*$^{+/-}$, *Nf1*$^{+/-}$ *Pak1*$^{-/-}$ and *Pak1*$^{-/-}$ mice. Using whole-cell patch clamp from BLA principal neurons, we studied spontaneous excitatory and inhibitory postsynaptic currents (sEPSCs and sIPSCs, respectively). Whereas pyramidal neurons of the BLA from *Nf1*$^{+/-}$ mice exhibited no differences in the amplitudes of either sIPSCs ($n = 4, 4, 3, 3$ mice per genotype and $n = 11, 11, 14, 14$ cells patched per genotype; no *Nf1*$^{+/-}$ × *Pak1*$^{-/-}$ interaction $F_{1,46} = 0.1$, $P = 0.77$; **Fig. 3a**,**b**) or miniature IPSCs (mIPSCs) (no *Nf1*$^{+/-}$ × *Pak1*$^{-/-}$ interaction $F_{1,46} = 0.3$, $P = 0.59$; **Fig. 3a**,**b**), they did show significant increases in the frequencies of both sIPSCs (*Nf1*$^{+/-}$ × *Pak1*$^{-/-}$ interaction $F_{1,46} = 6.11$, $P = 0.017$; **Fig. 3a**,**c**) and mIPSCs (*Nf1*$^{+/-}$ × *Pak1*$^{-/-}$ interaction $F_{1,46} = 9.21$, $P = 0.004$; **Fig. 3a**,**c**) compared to those from WT mice. Furthermore, deletion of Pak1 completely normalized the increase in frequency in *Nf1*$^{+/-}$ mice without affecting the amplitude of sIPSCs and mIPSCs in the amygdala neurons (**Fig. 3a**–**c**), confirming that Pak1 deletion also restores the increased BLA network inhibitory activity induced by *Nf1* mutation.

Next we analyzed both sEPSCs and mEPSCs from pyramidal neurons in the BLA of *Nf1*$^{+/-}$ mice and found significant increases in the frequency of sEPSCs (*Nf1*$^{+/-}$ × *Pak1*$^{-/-}$ interaction $F_{1,62} = 4.53$, $P = 0.037$) and mEPSCs (*Nf1*$^{+/-}$ × *Pak1*$^{-/-}$ interaction $F_{1,56} = 3.99$, $P = 0.05$) but not in the amplitude of sEPSCs (no *Nf1*$^{+/-}$ × *Pak1*$^{-/-}$ interaction $F_{1,62} = 2.68$, $P = 0.107$) or mEPSCs ($n = 4, 4, 3, 3$ mice per genotype and $n = 11, 11, 14, 14$ cells patched per genotype; no *Nf1*$^{+/-}$ × *Pak1*$^{-/-}$ interaction $F_{1,56} = 1.03$, $P = 0.314$; **Fig. 3d**–**f**). We detected additional significant increases in the amplitude of sEPSCs (*Pak1*$^{-/-}$ effect $F_{1,62} = 76.63$, $P < 0.0001$) and mEPSCs (*Pak1*$^{-/-}$ effect $F_{1,56} = 148.7$, $P < 0.0001$) in *Pak1*$^{-/-}$ and *Nf1*$^{+/-}$ *Pak1*$^{-/-}$ mice. These network changes suggest increases in presynaptic GABA release in the BLA of *Nf1*$^{+/-}$ mice, similar to findings in the hippocampus[16]. However, unlike in the hippocampus, there appeared to be additional changes in glutamate neurotransmission in the amygdalas of *Nf1*$^{+/-}$ mice.

To determine whether changes in synaptic plasticity within the amygdala might account for the social learning impairments of the *Nf1*$^{+/-}$ mutants, we examined LTP in BLA slices from these mice. Using a theta-burst stimulation (TBS) protocol[23], we elicited persistent potentiation of excitatory postsynaptic potentials (EPSPs) in WT mice that lasted at least 60 min after stimulation. In the *Nf1*$^{+/-}$ mice, although the initial potentiation was comparable to that in WT neurons, we observed a significant decay over the time ($n = 6, 6, 4, 4$ mice per genotype and $n = 7, 12, 8, 5$ cells patched per genotype;

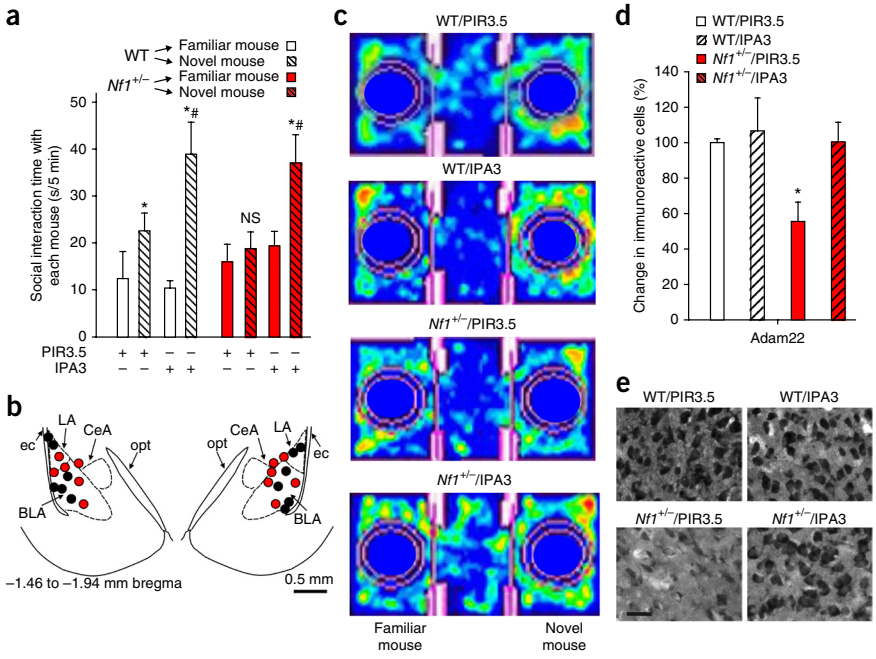

Figure 5 Amygdalar preinjection of Pak1 inhibitor restores long-term social behavioral deficits and normalizes local Adam22 expression in *Nf1*$^{+/-}$ mice. (**a**) Time spent in close proximity to either the novel or familiar mouse cage (≤2.5 cm from the wire cage). * indicates a novel mouse preference, and # indicates an enhanced social preference in WT mice and a rescue of social preference in *Nf1*$^{+/-}$ mice (side preference × *Nf1*$^{+/-}$ interaction, $P = 0.036$, and side preference × Pak1 inhibitor interaction, $P = 0.008$). NS, not significant. Graphs depict the mean ± s.e.m. (**b**) A coronal mouse brain section (taken from ref. 38) indicating the location of the injection sites (red circles) within the BLA from −1.46 to −1.94 mm bregma. ec, external capsule; LA, lateral amygdala; opt, optic tract. (**c**) Representative heat maps of the time spent in each region. The labels are shown as genotype/treatment in **c**–**e**. (**d**) Number of Adam22-immunoreactive cells in the BLA of WT and *Nf1*$^{+/-}$ mice treated with vehicle or IPA3 from the crossover experiment in **a**–**c**. Bars represent the mean, and error bars represent the s.e.m. * indicates a *Nf1*$^{+/-}$ effect, $P = 0.014$, and a Pak1 inhibitor effect, $P = 0.013$. (**e**) Photomicrographs of Adam22-immunoreactive cells in the BLA of WT and *Nf1*$^{+/-}$ mice treated with vehicle or IPA3. Scale bar, 25 μm. Statistical analyses in **a** were performed by two-way ANOVA with genotype and drug treatment as the main factors and side preference as a repeated measure, and those in **d** were performed by two-way ANOVA with genotype and drug treatment as the main factors.

Fig. 3g–i). By 50 min after stimulation, the amplitude of EPSPs was no longer significantly different from those recorded 5 min before TBS in *Nf1*$^{+/-}$ mice (*Nf1*$^{+/-}$ effect over time $F_{14,392} = 0.6$, $P = 0.838$). In contrast, LTP induced in *Nf1*$^{+/-}$ *Pak1*$^{-/-}$ mice was equivalent to that in the WT mice (genotype × time interaction $F_{42,392} = 3.2$, $P < 0.001$; **Fig. 3g–i**). The amplitude of the EPSPs induced by TBS in *Pak1*$^{-/-}$ mice was comparable to the amplitude of EPSPs recorded from BLA neurons of WT mice (*Pak1*$^{-/-}$ effect over time $F_{14,392} = 3.8$, $P < 0.001$; **Fig. 3g–i**). These results show that *Nf1*$^{+/-}$ mice had disrupted amygdala LTP and that Pak1 deletion can rescue these LTP deficits.

Pak1 deletion corrects altered amygdala synaptic proteins in *Nf1*$^{+/-}$ mice

We next used mass spectrometry to measure the expression levels of synaptic and neuronal proteins in the amygdalas of WT, *Nf1*$^{+/-}$, *Nf1*$^{+/-}$ *Pak1*$^{-/-}$ and *Pak1*$^{-/-}$ mice. We first identified proteins that were changed in *Nf1*$^{+/-}$ compared to WT mice and then determined which of those altered proteins were specifically restored in *Nf1*$^{+/-}$ *Pak1*$^{-/-}$ mice without being similarly altered by deletion of the Pak1 gene alone. The group of proteins thus identified would likely be the key to the disruption of the amygdala network observed in the *Nf1*$^{+/-}$ mice. On the basis of our selection algorithm, out of the 380 proteins measured, we identified only 3 in the BLA that met all three selection criteria, i.e., they were disrupted in *Nf1*$^{+/-}$ compared to WT mice (criteria one, 73 proteins; **Supplementary Table 1**), they were not changed in *Pak1*$^{-/-}$compared to WT mice (criteria 2), and they were rescued to near WT levels in *Nf1*$^{+/-}$ *Pak1*$^{-/-}$ mice ($n = 6, 6, 6, 6$; **Table 1**). There was a substantial, nearly 85% loss of Adam22 levels (*Nf1*$^{+/-}$ effect $F_{1,24} = 28.3$, $P < 0.001$ and *Pak1*$^{-/-}$ effect $F_{1,24} = 4.4$, $P = 0.048$; **Fig. 4a**), along with a 300% increase in the levels of cyclase-associated protein (Cap1) (*Nf1*$^{+/-}$ × *Pak1*$^{-/-}$ interaction $F_{1,23} = 10.0$, $P = 0.005$; **Fig. 4a**) and a 70% increase in Hsp70 levels (*Nf1*$^{+/-}$ × *Pak1*$^{-/-}$ interaction $F_{1,24} = 5.9$, $P = 0.025$; **Fig. 4b**) in the *Nf1*$^{+/-}$ mice, and all of these alterations were rescued by Pak1 deletion. Using immunocytochemistry, we further confirmed that there was a significant reduction in the number of Adam22-positive cells only ($n = 5, 7, 6, 6$; *Nf1*$^{+/-}$ effect $F_{1,24} = 7.1$, $P = 0.015$, *Pak1*$^{-/-}$ effect $F_{1,24} = 6.7$, $P = 0.018$; **Fig. 4c**,**f**), whereas the numbers of cells positive for Cap1 ($t_9 = -1.0$, $P = 0.337$) or Hsp70 ($t_9 = -0.3$, $P = 0.748$) were unaltered ($n = 4, 6$, with one outlier removed from WT group, and $n = 4, 7$, respectively; **Fig. 4d**,**e**) in the BLA of *Nf1*$^{+/-}$ mice compared to WT mice. This reduction in Adam22-positive cells was also rescued in the *Nf1*$^{+/-}$ *Pak1*$^{-/-}$ mice.

Local Pak1 inhibition in the amygdala also rescues deficits in *Nf1*$^{+/-}$ mice

Using constitutive gene deletion, one cannot definitively conclude that the social learning deficits are being rescued by selective Pak1 inhibition within the amygdala. Therefore, in a subsequent experiment, we tested the effects of bilaterally injecting previously known effective doses of a Pak1 inhibitor, IPA3 (or its inactive enantiomer PIR3.5 as control), into the BLA of *Nf1*$^{+/-}$ mice 30 min before assessment in the social familiarity test on days 1 and 2. Preinjection of IPA3 (100 μM, 100 nl), but not PIR3.5, into the BLA increased preference for the novel mouse in *Nf1*$^{+/-}$ mice during the long-term social memory test. Notably, IPA3 injection into the BLA also increased social preference in WT mice during the long-term social memory test to levels above baseline, further supporting a role of the BLA and Pak1 activity in social learning ($n = 6, 6, 6, 6$; side preference × *Nf1*$^{+/-}$ interaction $F_{1,18} = 5.2$, $P = 0.036$, and side preference × Pak1 inhibitor interaction $F_{1,18} = 8.8$, $P = 0.008$; **Fig. 5a–c**). Additionally, we also confirmed that there were reduced numbers of Adam22-immunoreactive cells in the BLA of *Nf1*$^{+/-}$ mice, an effect that was rescued in *Nf1*$^{+/-}$ mice pretreated with IPA3 in the BLA ($n = 3, 3, 3, 3$; *Nf1*$^{+/-}$ effect $F_{1,12} = 9.7$, $P = 0.014$, and Pak1 inhibitor effect $F_{1,12} = 10.0$, $P = 0.013$; **Fig. 5d**,**e**). To validate that the doses of IPA3 (and not those of the

inactive enantiomer PIR3.5) blocked Pak1 function in the amygdala, we tested the effects of preinjecting these drugs (100 μM, 100 nl) on the increases in the number of pErk-immunoreactive cells after stimulation with dimethylsulphoxide (DMSO), a known activator of Pak1 activity in neurons[24,25]. Injections of DMSO induced the increases in pErk expression in the amygdala, whereas preinjection with IPA3, but not PIR3.5, was able to block these effects (n = 5, 3, 4; $F_{2,11}$ = 22.6, P < 0.001; **Supplementary Fig. 2a**,**d**,**e**). Acute activation of Pak1 with injections of DMSO into the BLA of WT mice also caused a reduction in the number of Adam22-immunoreactive cells, and IPA3 (but not PIR3.5) preinjections blocked those reductions as well (n = 5, 3, 4; $F_{2,11}$ = 6.2, P = 0.020; **Supplementary Fig. 2b**,**d**,**e**).

DISCUSSION

In summary, our findings demonstrate that *Nf1*$^{+/-}$ mice exhibit a selective deficit in social learning, and the mechanisms underlying these social learning deficits appear to be disruption in the regulation of classical Mapk pathways in the amygdala. We also determined that *Nf1*$^{+/-}$ mice show disruptions of synaptic plasticity (LTP), GABA-mediated inhibition and glutamate excitation of neurons and altered expression of the important synaptic proteins Adam22, Cap1 and Hsp70 within the amygdala. ADAM22 is a synaptic protein that is thought to be critical for regulating the strength of glutamate neurotransmission and LTP and has been shown to specifically anchor AMPA receptors on the postsynaptic terminals in the hippocampus[26–28]. Therefore, although the role of ADAM22 in anchoring AMPA receptors in the amygdala specifically has not been demonstrated directly, significant decreases in Adam22 in *Nf1*$^{+/-}$ mice in the amygdala could be predicted to cause a similar failure to anchor AMPA receptors to the postsynaptic membrane and sustain LTP, as demonstrated in *Nf1*$^{+/-}$ mice (a hypothetical illustration is shown in **Supplementary Fig. 1b**). Similarly, HSP70 is thought to be critical for anchoring the GABA synthetic mechanisms to the presynaptic terminals[29], and increases in the expression levels of HSP70 could lead to increases in presynaptic GABA release specifically and an increased frequency of sIPSCs, as we demonstrated here. These increases in GABA release may also compensate for some of the glutamate neurotransmission disequilibrium and could be a potential explanation for *Nf1*$^{+/-}$ mice not developing the severe seizures that are seen in *Adam22*$^{-/-}$ mice[30]. CAP1 is a protein that has an important role in the regulation of actin polymerization and synaptic remodeling, processes that are critical for long-term memory[31].

The social deficits and all of the aforementioned amygdala disruptions in *Nf1*$^{+/-}$ mice were rescued by deletion of *Pak1* gene. Pharmacological blockade of Pak1 function within the amygdala also rescued the social deficits seen in *Nf1*$^{+/-}$ mice. These results suggest that Pak1 inhibition, consistent with the recently reported reductions in neurofibroma tumors in children with NF1 (ref. 32), may be a therapeutic target of interest for the treatment of NF1-related social and learning symptoms that pose a major burden to affected children[1,32]. Deletion of Pak1 gene, which rescued the behavioral deficits seen in *Nf1*$^{+/-}$ mice, also restored the changes in synaptic protein expression and, as predicted by our hypotheses, rescued the network disruptions in the amygdala and normalized amygdala LTP. The precise mechanisms involved in these gene expression changes induced by *Nf1* haploinsufficiency and their rescue by Pak1 deletion have yet to be determined. However, there is supportive evidence that inhibiting Pak1 levels will reduce CAP1 levels in the CNS[33], and the genes for Pak1, Erk1 and Lgl-4 (the endogenous CNS ligand for Adam22) are all located on mouse chromosome 7. Moreover, it has been shown that single injection of a Pak1 inhibitor completely rescues seizures and behavioral abnormalities, such as hyperactivity and repetitive movements, in fragile X mental retardation 1 (*Fmr1*$^{-/-}$) mice[34]. Because of increases in the co-occurrence of NF1 and ASDs[35,36], these findings may also have important implications regarding the molecular targets for the remediation of social deficits in some forms of ASD. Indeed, a recent deep-brain stimulation report showed that stimulating the BLA region directly in a severely autistic child was effective in improving core symptoms of the ASD in the emotional, social and even cognitive domains over a follow-up period of 24 months[37]. In conclusion, we have demonstrated selective deficits in social learning and underlying disruptions in the amygdala network caused by a single-gene (*Nf1*) mutation. We have also provided a potential new therapeutic approach toward ameliorating these disabling behavioral symptoms in patients with NF1 and some forms of ASD.

METHODS

Methods and any associated references are available in the online version of the paper.

Note: Any Supplementary Information and Source Data files are available in the online version of the paper.

ACKNOWLEDGMENTS

This work was supported by grants from the National Center for Advanced Translational Sciences, US National Institutes of Health UL1RR025761/TR000006, R01 MH52619 and MH065702 (to A.S.), a predoctoral fellowship to J.P.S. (TL1 RR 025759), K01AG044466 (to P.L.J.) and R01 CA74177-06 (to D.W.C.). We thank T. Jacks (Massachusetts Institute of Technology) for providing *Nf1*$^{+/-}$ mice and J. Chernoff (Fox Chase Cancer Center) for providing *Pak1*$^{-/-}$ mice.

AUTHOR CONTRIBUTIONS

A.S., along with A.I.M., P.L.J., J.P.S. and D.W.C., formulated the hypotheses and designed the studies. S.-J.P. and D.W.C. maintained the mouse colony and genotyped all mice. J.P.S. and S.P.J. performed the behavioral assays shown in **Figure 1**, and J.P.S. performed those shown in **Figure 2**. For **Figure 1** and **Supplementary Figure 3**, western blots were performed by R.K. and W.Z., and immunohistochemistry was performed by L.M.F. and P.L.J. A.I.M. performed all electrophysiology experiments shown in **Figure 3**. For **Table 1** and **Figure 4a**,**b** and **Supplementary Table 1**, A.I.M. micropunched the BLA, Y.S.M. and Z.M.S. conducted the proteomics assay, and C.G., L.L. and P.L.J. analyzed the data. The immunohistochemistry shown in **Figure 4c**–**f** was performed by L.M.F. and P.L.J. The stereotaxic surgeries and behavioral assays shown in **Figure 5** were performed by D.A. and C.B. The stereotaxic surgeries and immunohistochemistry shown in **Supplementary Figure 2** were done by D.A. and P.L.J. A.I.M. and P.L.J. analyzed data and created figures. A.I.M., P.L.J., J.P.S., D.W.C. and A.S. interpreted the data and collectively wrote the main draft of the article, with all other authors contributing to the revisions, and all authors approved of the final version.

COMPETING FINANCIAL INTERESTS

The authors declare no competing financial interests.

1. Johnson, N.S., Saal, H.M., Lovell, A.M. & Schorry, E.K. Social and emotional problems in children with neurofibromatosis type 1: evidence and proposed interventions. *J. Pediatr.* **134**, 767–772 (1999).
2. Barton, B. & North, K. Social skills of children with neurofibromatosis type 1. *Dev. Med. Child Neurol.* **46**, 553–563 (2004).
3. Noll, R.B. *et al.* Social, emotional, and behavioral functioning of children with NF1. *Am. J. Med. Genet. A.* **143A**, 2261–2273 (2007).
4. Lehtonen, A., Howie, E., Trump, D. & Huson, S.M. Behaviour in children with neurofibromatosis type 1: cognition, executive function, attention, emotion, and social competence. *Dev. Med. Child Neurol.* **55**, 111–125 (2013).
5. Huijbregts, S.C. & de Sonneville, L.M. Does cognitive impairment explain behavioral and social problems of children with neurofibromatosis type 1? *Behav. Genet.* **41**, 430–436 (2011).
6. Huijbregts, S., Jahja, R., De Sonneville, L., de Breij, S. & Swaab-Barneveld, H. Social information processing in children and adolescents with neurofibromatosis type 1. *Dev. Med. Child Neurol.* **52**, 620–625 (2010).
7. Garg, S. *et al.* Neurofibromatosis type 1 and autism spectrum disorder. *Pediatrics* **132**, e1642–e1648 (2013).

8. Garg, S. *et al.* Autism and other psychiatric comorbidity in neurofibromatosis type 1: evidence from a population-based study. *Dev. Med. Child Neurol.* **55**, 139–145 (2013).
9. Walsh, K.S. *et al.* Symptomatology of autism spectrum disorder in a population with neurofibromatosis type 1. *Dev. Med. Child Neurol.* **55**, 131–138 (2013).
10. Pride, N.A. *et al.* The genetic and neuroanatomical basis of social dysfunction: lessons from neurofibromatosis type 1. *Hum. Brain Mapp.* **35**, 2372–2382 (2014).
11. Truitt, W.A. *et al.* From anxiety to autism: spectrum of abnormal social behaviors modeled by progressive disruption of inhibitory neuronal function in the basolateral amygdala in Wistar rats. *Psychopharmacology (Berl.)* **191**, 107–118 (2007).
12. Maaswinkel, H., Baars, A.M., Gispen, W.H. & Spruijt, B.M. Roles of the basolateral amygdala and hippocampus in social recognition in rats. *Physiol. Behav.* **60**, 55–63 (1996).
13. Todd, R.M. & Anderson, A.K. Six degrees of separation: the amygdala regulates social behavior and perception. *Nat. Neurosci.* **12**, 1217–1218 (2009).
14. Zhu, Y., Ghosh, P., Charnay, P., Burns, D.K. & Parada, L.F. Neurofibromas in NF1: Schwann cell origin and role of tumor environment. *Science* **296**, 920–922 (2002).
15. Costa, R.M. *et al.* Mechanism for the learning deficits in a mouse model of neurofibromatosis type 1. *Nature* **415**, 526–530 (2002).
16. Cui, Y. *et al.* Neurofibromin regulation of ERK signaling modulates GABA release and learning. *Cell* **135**, 549–560 (2008).
17. Sankoorikal, G.M., Kaercher, K.A., Boon, C.J., Lee, J.K. & Brodkin, E.S. A mouse model system for genetic analysis of sociability: C57BL/6J versus BALB/cJ inbred mouse strains. *Biol. Psychiatry* **59**, 415–423 (2006).
18. Crawley, J.N. *et al.* Social approach behaviors in oxytocin knockout mice: comparison of two independent lines tested in different laboratory environments. *Neuropeptides* **41**, 145–163 (2007).
19. Brittain, J.M. *et al.* Suppression of inflammatory and neuropathic pain by uncoupling CRMP-2 from the presynaptic Ca^{2+} channel complex. *Nat. Med.* **17**, 822–829 (2011).
20. Le, L.Q. & Parada, L.F. Tumor microenvironment and neurofibromatosis type I: connecting the GAPs. *Oncogene* **26**, 4609–4616 (2007).
21. Wang, Y. *et al.* ERK inhibition rescues defects in fate specification of Nf1-deficient neural progenitors and brain abnormalities. *Cell* **150**, 816–830 (2012).
22. Zhang, Y.Y. *et al.* Nf1 regulates hematopoietic progenitor cell growth and ras signaling in response to multiple cytokines. *J. Exp. Med.* **187**, 1893–1902 (1998).
23. Li, C., Dabrowska, J., Hazra, R. & Rainnie, D.G. Synergistic activation of dopamine D1 and TrkB receptors mediate gain control of synaptic plasticity in the basolateral amygdala. *PLoS ONE* **6**, e26065 (2011).
24. Deacon, S.W. *et al.* An isoform-selective, small-molecule inhibitor targets the autoregulatory mechanism of p21-activated kinase. *Chem. Biol.* **15**, 322–331 (2008).
25. Kalwat, M.A., Yoder, S.M., Wang, Z. & Thurmond, D.C. A p21-activated kinase (PAK1) signaling cascade coordinately regulates F-actin remodeling and insulin granule exocytosis in pancreatic β cells. *Biochem. Pharmacol.* **85**, 808–816 (2013).
26. Fukata, Y. *et al.* Epilepsy-related ligand/receptor complex LGI1 and ADAM22 regulate synaptic transmission. *Science* **313**, 1792–1795 (2006).
27. Ohkawa, T. *et al.* Autoantibodies to epilepsy-related LGI1 in limbic encephalitis neutralize LGI1-ADAM22 interaction and reduce synaptic AMPA receptors. *J. Neurosci.* **33**, 18161–18174 (2013).
28. Fukata, Y. *et al.* Disruption of LGI1-linked synaptic complex causes abnormal synaptic transmission and epilepsy. *Proc. Natl. Acad. Sci. USA* **107**, 3799–3804 (2010).
29. Hsu, C.C. *et al.* Association of l-glutamic acid decarboxylase to the 70-kDa heat shock protein as a potential anchoring mechanism to synaptic vesicles. *J. Biol. Chem.* **275**, 20822–20828 (2000).
30. Sagane, K. *et al.* Ataxia and peripheral nerve hypomyelination in ADAM22-deficient mice. *BMC Neurosci.* **6**, 33 (2005).
31. Hubberstey, A.V. & Mottillo, E.P. Cyclase-associated proteins: CAPacity for linking signal transduction and actin polymerization. *FASEB J.* **16**, 487–499 (2002).
32. Yang, F.C. *et al.* Nf1-dependent tumors require a microenvironment containing $Nf1^{+/-}$ and c-kit–dependent bone marrow. *Cell* **135**, 437–448 (2008).
33. Nakatani, N. *et al.* Expression analysis of actin-related genes as an underlying mechanism for mood disorders. *Biochem. Biophys. Res. Commun.* **352**, 780–786 (2007).
34. Dolan, B.M. *et al.* Rescue of fragile X syndrome phenotypes in Fmr1 KO mice by the small-molecule PAK inhibitor FRAX486. *Proc. Natl. Acad. Sci. USA* **110**, 5671–5676 (2013).
35. Martin, I. *et al.* Transmission disequilibrium study of an oligodendrocyte and myelin glycoprotein gene allele in 431 families with an autistic proband. *Neurosci. Res.* **59**, 426–430 (2007).
36. Marui, T. *et al.* Association between the neurofibromatosis-1 (NF1) locus and autism in the Japanese population. *Am. J. Med. Genet. B Neuropsychiatr. Genet.* **131B**, 43–47 (2004).
37. Sturm, V. *et al.* DBS in the basolateral amygdala improves symptoms of autism and related self-injurious behavior: a case report and hypothesis on the pathogenesis of the disorder. *Front. Hum. Neurosci.* **6**, 341 (2012).
38. Paxinos, G. & Franklin, K.B.J. *The Mouse Brain in Stereotaxic Coordinates* (Academic Press, 2008).

ONLINE METHODS

Animals. Most experiments were conducted using adult male mice, except for the cellular assay and western blotting experiment, which was done using mice at postnatal day (P) 2–3, and the electrophysiology experiments, which were done in 2- to 3-month-old mice. The mouse strains tested were bred on a C57BL/6J background and included WT, *Nf1*$^{+/-}$, *Nf1*$^{+/-}$ *Pak1*$^{-/-}$ and *Pak1*$^{-/-}$. The *Nf1*$^{+/-}$ mice were obtained from T. Jacks at the Massachusetts Institute of Technology (Cambridge, MA), and *Pak1*$^{-/-}$ mice were obtained from J. Chernoff (Fox Chase Cancer Center). To generate the *Nf1*$^{+/-}$ *Pak1*$^{-/-}$ mice, *Pak1*$^{-/-}$ mice were intercrossed with the *Nf1*$^{+/-}$ strain. All mice were singly housed, given food and water *ad libitum* and maintained on a 12-h light, 12-h dark cycle (7 a.m./7 p.m.) at 72 °F. Animal care procedures were conducted in accordance with the US National Institutes of Health (NIH) Guidelines for the Care and Use of Laboratory Animals (NIH publication number 80-23) revised 1996. All procedures were approved by the Indiana University School of Medicine Institutional Animal Care and Use Committee (protocol number 10326).

Behavioral testing. The behavioral testing reported in **Figure 1a–d** and **g–j** was done in the same cohort of mice, which were tested in the social behavior test on day 1, the elevated plus maze (**Fig. 1g**) on day 2, the olfactory test on day 3 and the behavioral despair test on day 4. The behavioral testing reported in **Figure 1e**,**f** was in done in the same cohort of mice, which were tested in the novel object recognition test on day 1 and the passive avoidance test on day 2. The behavioral testing reported in **Figure 2b–h** was done in the same cohort of mice, which were tested in the social behavior test on day 1, the elevated plus maze (**Fig. 1g**) on day 2, the olfactory test on day 3 and the behavioral despair test on day 4. The social behavior tests reported in **Figure 4** were done in a separate cohort of mice in a crossover design with 5 d between crossover. All behavioral tests were videotaped and independently scored at a later time by two individuals who were unaware of the animals' genotype. After each test, the apparatus were cleaned with 90% ethanol and dried.

Social behavior tests. The social interaction test was conducted as previously described[17,18]. Four 10-min sessions were conducted, including (i) day 1: acclimation (two empty cylindrical cages); (ii) day 1: 5 min after acclimation, assessing preference for social interaction (novel mouse (mouse 1) and an empty cage); (iii) day 1: 5 min after initial exposure to mouse 1, a short-term social learning test was done with mouse 1 (the now familiar mouse) and mouse 2 (a novel mouse); and (iv) long-term social learning 24 h later (familiar mouse (mouse 2) and a novel mouse (mouse 3)). After the short-term social learning session, the novel mouse was removed from the apparatus, and the test mouse was allowed to interact with the familiar mouse for an additional 45 min. The stimulus mice used for the social behavior tests were age-matched, adult male C57BL/6J mice that had no previous contact with the test mice.

Novel object recognition test. The novel object recognition test was used to measure short-term memory retention. The apparatus consisted of an opaque Plexiglas chamber of (50 cm × 50 cm × 50 cm). Two objects with similar textures, colors and sizes (two cylinders) were placed in opposite corners of the chamber. Between trials, the objects and the box were cleaned with 70% ethanol. The habituation session consisted of placing a mouse in the chamber for 10 min, and at the end of each session, the mouse was returned to the home cage. Two hours later, the mouse was placed in the chamber with a similar cylinder in each corner, and the time exploring the two objects (measured as the mouse's nose within 1 inch of the object) was assessed for 10 min. 30 min later, the mouse was placed in the chamber with the now-familiar cylinder and an unfamiliar cube in each corner. The time exploring the two dissimilar objects (again measured as the mouse's nose within 1 inch of the object) was assessed for 10 min.

Passive avoidance memory test. This passive avoidance task is a one-trial fear-motivated avoidance task in which the mouse learns to refrain from stepping from a lighted chamber through a door to an apparently safer enclosed dark chamber where the mouse previously received a shock. The training chambers consist of one compartment (20 cm × 40 cm × 30 cm height) that is lighted by an overhead stimulus light (40 W bulb) and a second compartment (20 cm × 20 cm × 30 cm height) that is black and enclosed so as to remain dark. An automatic guillotine door separates the two compartments.

On habituation day, the mouse is placed in a lighted compartment facing away from the dark compartment, allowed to explore for 30 s and then the door to the dark chamber is raised. When the mouse enters the dark compartment, the guillotine door is closed. 5 min later, the mouse is removed and returned to the home cage. On the training day, the test is repeated, except that after entering the dark chamber, the door is closed and the mouse receives a foot shock (0.5 mA, 2-s duration) through a grid. 30 s after the foot shock, the mouse is returned to the home cage. On testing day, the test is repeated, and the latency to enter the dark chamber with front two paws is determined.

Elevated plus maze. The elevated plus maze was conducted as described previously[19], where mice were allowed to freely explore the entire apparatus for 5 min. This procedure was again performed 24 h later as a measure of avoidance learning. An arm entry was defined as having all four paws into the arm of the elevated plus maze.

The Porsolt forced swim test. The forced swim test was used to measure aspects of behavioral despair[19,39]. The forced swim apparatus consisted of a cylindrical chamber constructed of clear Plexiglas with a diameter of 8.5 inches and height of 10 inches. For each trial, the chamber was filled with 25 ± 1 °C water. The test mouse was then gently placed into the cylinder for 15 min. Twenty-four hours later, the mice were re-exposed to the same conditions for an additional 6-min trial. Immobility was considered as the cessation of limb movements except for minor involuntary hindlimb movements.

Olfactory habituation test. The mice were placed in a clean cage and were assessed for time spent sniffing cotton-tipped swabs suspended from the cage lid. The cotton swabs were dipped in water or almond extract (1:100 dilution) or were wiped in a zigzag pattern across the bottom surface of a cage that contained an unfamiliar mouse (a singly housed C57BL/6J male mouse). The sequences of three identical swabs were assayed for each odor as follows: water, water, water, almond, almond, almond, unfamiliar cage, unfamiliar cage, unfamiliar cage. Each swab was presented for 2 min for a total session lasting 18 min per mouse.

Isolation and culture of neuronal cells from mouse strains. Neurons were obtained from the frontal cortical and amygdala regions of P2–P3 mice that were aseptically dissected and cultured from each genotype (WT, *Nf1*$^{+/-}$, *Nf1*$^{+/-}$ *Pak1*$^{-/-}$ and *Pak1*$^{-/-}$). After dissection of each brain region, neuronal cells were isolated by dissociation both enzymatically and mechanically (by trituration through a flame-polished Pasteur pipette) in a Papain solution (12 units/ml; Worthington) as described previously[19]. For this experiment, the neuronal cultures were assigned to one of two experimental conditions: (i) at basal levels or (ii) after the application of recombinant mouse SCF (PreproTech) at 10 ng/ml. SCF was applied to the neuronal cultures for 2 min. The cells were then washed with ice-cold PBS and lysed in buffer, as described below.

Immunoblotting Erk and pErk in mouse cortical and amygdala neurons. Whole-cell protein extracts were obtained from the frontal cortical and amygdala regions of P2–P3 mice and placed in lysis buffer (50 mM Tris, pH 7.4, 150 mM NaCl, 2 mM ethylenediaminetetraacetic acid (EDTA), pH 8.0, 1% Triton X-100, 1 mM phenylmethylsulfonyl fluoride (PMSF), 1 mM NaF, 1 mM Na_3VO_4, 10% glycerol and protease inhibitors). The samples were sonicated, and cellular debris was removed by centrifugation at 13,000*g* for 30 min at 4 °C. Protein concentrations were determined using a bicinchoninic acid (BCA) assay (Thermo Scientific). Equivalent amounts of protein were electrophoresed on 10% sodium dodecyl sulfate polyacrylamide gel electrophoresis (SDS-PAGE) gels, transferred to polyvinylidene difluoride (PVDF) membranes (GE Healthcare, Little Chalfont, UK) and detected by western blotting using the ECL Plus system (Amersham Biosciences). The antibodies used were to pErk1/2 (4370, 1:1,000 dilution, Cell Signaling Technology), Erk1/2 (4695, 1:1,000 dilution, Cell Signaling Technology) and GAPDH (MAB374, 1:1,000 dilution, Millipore). Cell Signaling reports that the Erk1/2 monoclonal antibody p44/42 MAP kinase (137F5) rabbit monoclonal antibody detects endogenous levels of total p44/42 MAP kinase (Erk1/Erk2) protein. The antibody does not crossreact with JNK/SAPK or p38 MAP kinase, and the monoclonal antibody to pErk1/2 is produced by immunizing rabbits with a synthetic phosphopeptide corresponding to residues surrounding Thr202 and Tyr204 of human p44 MAP kinase and binds to endogenous levels of p44 and p42

MAP kinase (Erk1 and Erk2) when dually phosphorylated at Thr202 and Tyr204 of Erk1 (Thr185 and Tyr187 of Erk2) and singly phosphorylated at Thr202. This antibody does not crossreact with the corresponding phosphorylated residues of either JNK/SAPK or p38 MAP kinases. All mice were delivered to R.K., who was unaware of the animals' genotype.

Immunostaining of pErk in cells from the amygdala of mice exposed to a novel mouse. WT and *Nf1*$^{+/-}$ mice were habituated to the social learning apparatus with two empty cages and were placed in a social learning apparatus with a novel mouse in one cage 24 h later. Mice were then placed in the home cage for 80 min, anesthetized with isoflurane and then perfused transcardially with 250 ml 0.1 M PBS, followed by 250 ml of 0.1 M PB containing 4% paraformaldehyde and 3% sucrose and processed for immunohistochemistry to yield four alternative sets of serial coronal sections (30 µm). A standard immunohistochemical procedure was then performed as described in detail previously[40] using a monoclonal rabbit pErk1/2 antibody (1:200 dilution, 4370, Cell Signaling).

Protein expression analysis. Tissue slices were homogenized in 50 mM ammonium bicarbonate, and whole-cell protein extracts were obtained from brain slices in lysis buffer (30 mM Tris, pH 7.4, 150 mM NaCl, 1% Triton X-100, 0.1% SDS, 1 mM PMSF, 10 mM EDTA, 1 mM Na_2CO_3, 160 mM NaF and complete protease inhibitor) with a ProteoSpin total protein detergent clean up micro kit (Norgen, Canada). The BCA Protein Assay Kit (Pierce, Rockford, IL) was used to determine protein concentrations of the lysates (Pierce, Rockford, IL). Protein samples were reduced using dithiothreitol (DTT), and alkylation was achieved by adding iodoacetic acid (IAA). The protein samples then subjected to tryptic digestion at 37 °C overnight and quenched through the addition of neat formic acid. Liquid chromatography–tandem mass spectrometry (LC-MS/MS) analyses of the tryptic digests were performed using a Dionex 3000 Ultimate nano-LC system (Dionex, Sunnyvale, CA) interfaced to an LTQ Orbitrap hybrid mass spectrometer (Thermo Scientific, San Jose, CA). Prior to separation, a 2-µl aliquot of trypsin digestion (1.5 µg protein equivalent) was loaded on a PepMap300 C18 cartridge (5 µm, 300 Å; Dionex) and eluted through the analytical column (150 mm × 100 µm inner diameter, 200-Å pores) packed with C18 magic (Michrom Bioresources, Auburn, CA). Peptides originating from protein tryptic digests were separated using a reversed-phase gradient from 3–55% B, 99.9% acetonitrile with 0.1% formic at a 500 nl/min flow rate and passed through an ADVANCE ionization source (Michrom Bioresources, Auburn, CA). Switching between MS scan and collision-induced dissociation MS (CID-MS), eluted LC products undergo an initial full-spectrum MS scan from *m/z* 300 to *m/z* 2,000 in the Orbitrap at 15,000 mass resolutions. Subsequently CID-MS (at 35% normalized collision energy) was performed. The total cycle (six scans) is continuously repeated for the entire LC-MS run under data-dependent conditions. Mascot version 2.1.3 was used for all search results against the Swiss-Prot database for house mouse, and the quantitative analysis of proteins was carried out using the ProteinQuant Suit developed at Indiana University. The combined master files were then incorporated with their corresponding mzXML files and were submitted to ProteinQuant as described previously[41]. Pathway analyses were then conducted on proteins that showed significant differences between WT and *Nf1*$^{+/-}$ and that were restored in the *Nf1*$^{+/-}$ *Pak1*$^{-/-}$ genotype using INGENUITY systems software (Redwood City, CA). Protein expression data were further analyzed using one-way and two-way ANOVA. All mouse tissue was given to the proteomics core collaborators, who were unaware of the animals' genotype.

Electrophysiology. The electrophysiological recordings were performed in 2- to 3-month-old mice as described previously[42]. Briefly, after decapitation, the brains were rapidly removed and placed in oxygenated artificial cerebrospinal fluid (ACSF) (130 mM NaCl, 3.5 mM KCl, 1.1 mM KH_2PO_4, 1.3 mM $MgCl_2$, 2.5 mM $CaCl_2$, 30 mM $NaHCO_3$ and 10 mM glucose), and coronal slices (350 µM) were prepared containing the BLA. After an initial incubation of at least 30 min at 30 °C in oxygenated ACSF, slices were transferred to a recording chamber mounted on the stage of a Nikon E600FN Eclipse (Nikon Instruments, Melville, NY) microscope and perfused with ACSF (2–3 ml per minute) heated to 30 °C. Whole-cell patch-clamp recordings were obtained using standard techniques. Borosilicate glass electrodes (WPI, Sarasota, FL) (resistance 3–6 MΩ) were prepared with a potassium gluconate–based recording solution (130 mM K-gluconate, 3 mM KCl, 3 mM $MgCl_2$, 5 mM phosphocreatine, 2 mM K-ATP, 0.2 mM NaGTP and 10 mM 4-(2-hydroxyethyl)-1-piperazineethanesulfonic acid (HEPES)) and were maintained at a holding potential of −60 mV. BLA pyramidal neurons were identified according to their characteristic size and shape[43]. At the start of each experiment, except for the LTP experiments, a series of current clamp protocols was performed to further validate the identity of the BLA projection neurons. Drugs were added directly into the ACSF at the required concentration. The sIPSCs and mIPSCs (in the presence of 1 µM tetrodotoxin (TTX)) were recorded at a holding potential of −55 mV in the presence of 6,7-dinitroquinoxaline-2,3-dione (DNQX, 20 µM) and 3-(2-carboxypiperazin-4-yl)-propyl-1-phosphonic acid (CPP, 1 µM). The sEPSCs and mEPSCs (in 1 µM TTX) were acquired at a holding potential of −60 mV in the presence of the $GABA_A$ antagonist bicuculline methochloride (10 µM) and the $GABA_B$ antagonist 3-[[(3,4-dichlorophenyl)methyl]amino] propyl] diethoxymethyl)phosphinic acid (CGP52432, 1 µM). The spontaneous and miniature currents were captured continuously for 1 min and detected and analyzed afterwards using the MiniAnalysis (Synaptosoft, Decatur, GA).

EPSPs onto BLA projection neurons were evoked in a current clamp as described previously[23]. The $GABA_B$ antagonist CGP52432 (1 µM) was added to the ACSF, and the $GABA_A$ antagonist picrotoxin (50 µM) was included in the recording solution. The holding potential was adjusted to −70 mV, except during TBS, when the potential was adjusted to −55 mV to facilitate spike firing. A 10-min baseline period was recorded in each experiment, and recordings were continued for at least 60 min after LTP induction. The TBS was 40 ms in duration, with 100 bursts delivered at 5 Hz for 5 s (100 pulses total). Evoked postsynaptic potentials were analyzed using pClamp 10.3 (Molecular Devices, Sunnyvale, CA). All chemicals, except CPP and CGP52432 (Tocris Biosciences, Ellisville, MO), were purchased from Sigma-Aldrich (St. Louis, MO). All mice were brought to A.I.M., who was unaware of the animals' genotype.

Immunohistochemistry for Adam22, Cap1 and Hsp70 in the BLA. Mice were anesthetized with halothane then perfused transcardially with 250 ml 0.1 M PBS, followed by 250 ml of 0.1 M PB containing 4% paraformaldehyde and 3% sucrose and processed for standard immunohistochemistry as described in detail previously[40]. Here we used the following antibodies on separate serial sections: affinity purified rabbit anti-Adam22 polyclonal antibody (1:200 dilution, ab56122, Abcam, Cambridge, MA), rabbit anti-Cap1 polyclonal antibody (1:200 dilution, sc134637, Santa Cruz Biotechnology, Santa Cruz CA) and affinity purified rabbit anti-Hsp70 polyclonal antibody (1:100 dilution, NBP1-00880, Novus Biologicals, Littleton, CO). Abcam reports the following: the Adam22 immunogen was a synthetic peptide based on the metalloproteinase domain of human ADAM22, and the Adam22 antibody is reactive with mouse Adam22 protein at the predicted band in western blots. Santa Cruz reports that the Cap1 rabbit polyclonal antibody was raised against amino acids 14–74 mapping near the N terminus of CAP1 of human origin and is reactive with mouse Cap1 protein at the predicted band in western blots. Novus Biologicals reports that the Cap1 antibody was raised against the synthetic peptide corresponding to the residues surrounding Phe245 of human HSP70 and is reactive with mouse Hsp70 protein at the predicted band in western blots.

Photography and cell counts. Photomicrographs were obtained using a Leica brightfield microscope using N plan 5×, 10×, 20× and 40× objective lenses (model DMLB, Leica Microsystems), a SPOT digital camera (RT color, Diagnostics Instruments Inc., Sterling Heights, MI) and SPOT 4.7.1.32 for Windows digital imaging software. Photographic plates were prepared in CorelDraw X5 for Windows (Eden Prairie, MN). Immunoreactive cells in the BLA were counted on a 400× magnification photomicrograph and then verified at 400× using a Leica DMLB binocular microscope (Leica Microsystems) by an investigator (P.L.J.) who was blind to the experimental treatment of each animal.

Site-directed injections of a Pak1 inhibitor into the BLA of *Nf1* mice. *Stereotaxic cannula placement.* Prior to and during surgery, mice were anesthetized with a nose cone connected to an isoflurane system (MGX Research Machine, Vetamic) and placed in an ultraprecise stereotaxic apparatus for rodents (900 series Ultraprecise Kopf Instruments). Bilateral injection cannulae (26 gauge; Plastics One) were implanted into the BLA (anteroposterior (AP): −1.5, mediolateral (ML): ±3.35, dorsoventral (DV): −4.55, and the incisor bar was set at −3.0 mm to keep the lambda and bregma suture at the same DV) according to a standard stereotaxic atlas of the mouse brain[38]. The cannulae were secured to

doi:10.1038/nn.3822

the skull with three stainless steel screws (2.8 mm; Plastic One, Roanoke, VA) and Loctite adhesive. After completion of surgery, a dummy cannula that went the length of the guide was screwed in place. All mice then received buprenex at 1 mg per kg body weight subcutaneously and were placed on a warming pad until they had fully recovered.

Intracranial injection procedures. At 30 min before the novel mouse exposure and the long-term social memory testing the next day, WT and $Nf1^{+/-}$ mice received microinjections with an injector (33 gauge; Plastic Products) that fit into, and extended 0.5 mm beyond, the guide cannula. A 10-µl Hamilton syringe was placed on an infusion pump (Harvard Apparatus, Holliston, MA, model PHD 2000) and connected to the injection cannula using polyethylene (PE 50) tubing. The pump delivered 100 nl of either the Pak1 inhibitor IPA3 (3622, Tocris Biosciences; $n = 6$) or the inactive enantiomer PIR3.5 (4212, Tocris Biosciences; $n = 6$) dissolved in DMSO into the BLA per site over 30 s. The injection cannula remained in place for an additional minute to ensure complete delivery of the solution, and proper flow was confirmed in the cannulae after removal. All injection sites were verified using a 400×-magnification Leica DMLB brightfield microscope.

Statistical analyses of data. For the behavior tests shown in **Figure 1** with western blotting and immunohistochemistry with WT and $Nf1^{+/-}$ mice, data were analyzed using one-way ANOVA with genotype as the main factor and, when applicable, a side preference or time as a repeated measure. For the behavior tests shown in **Figure 2** with $Nf1^{+/-}$, $Nf1^{+/-}$ $Pak1^{-/-}$ and $Pak1^{-/-}$ mice, data were analyzed using one-way ANOVA with genotype as the main factor and, when applicable, a side preference or time as a repeated measure. For the electrophysiology experiments shown in **Figure 3**, the proteomics and immunohistochemistry analyses in **Table 1** and **Figure 4** and the behavior tests in **Figure 5** with WT, $Nf1^{+/-}$, $Nf1^{+/-}$ $Pak1^{-/-}$ and $Pak1^{-/-}$ mice, data were analyzed using two-way ANOVA with $Nf1^{+/-}$ and $Pak1^{-/-}$ as the main factors or genotype and drug treatment as the main factors and, when applicable, a side preference or time as a repeated measure. Significant effects were further analyzed using *post-hoc* Fisher's protected least significant difference (FLSD) tests for between-subjects effects of multiple groups or a two-way paired or independent *t* test (as appropriate) for two-group comparisons. A Dunnett's *post-hoc* test was used to compare the within-subject over-time effects shown in **Figure 3**. A Levene's test was conducted before analyses to assess for equality of variance. To protect against type 1 errors, the *n* numbers per group were considered acceptable if they were significant ($P < 0.05$) in the previously mentioned analyses. In cases where there was a trend toward significance ($P > 0.05$–0.060), power analyses were done to determine if the *n* numbers per group were sufficiently powered and to protect against type 2 errors. An outlier was detected for one animal in the behavioral assessments shown in **Figure 1c** and also in **Figure 5a** with a Grubb's test, and data from this animal were therefore excluded from analyses. There were no missing data for cell assays, western blots, proteomics analyses or electrophysiology. For proteomics analyses, using Pathway analyses in INGENUITY software, there were no missing data points. However in a subsequent secondary analyses using one-way ANOVA, there was one missing data point in the Cap1 WT group because of an outlier that was >2 s.d. from the mean (**Fig. 4a**). For immunohistochemistry, one data point was missing in the Cap1 WT group (**Fig. 4d**) and the Hsp70 $Nf1^{+/-}$ group (**Fig. 4e**) because there was no representative coronal slice containing the amygdala at that level of bregma, and another data point in the Cap1 WT group was an outlier.

39. Porsolt, R.D., Le Pichon, M. & Jalfre, M. Depression: a new animal model sensitive to antidepressant treatments. *Nature* **266**, 730–732 (1977).
40. Johnson, P.L., Truitt, W.A., Fitz, S.D., Lowry, C.A. & Shekhar, A. Neural pathways underlying lactate-induced panic. *Neuropsychopharmacology* **33**, 2093–2107 (2008).
41. Mann, B. *et al.* ProteinQuant Suite: a bundle of automated software tools for label-free quantitative proteomics. *Rapid Commun. Mass Spectrom.* **22**, 3823–3834 (2008).
42. Molosh, A.I. *et al.* NPY Y1 receptors differentially modulate $GABA_A$ and NMDA receptors via divergent signal transduction pathways to reduce excitability of amygdala neurons. *Neuropsychopharmacology* **38**, 1352–1364 (2013).
43. McDonald, A.J., Mascagni, F., Mania, I. & Rainnie, D.G. Evidence for a perisomatic innervation of parvalbumin-containing interneurons by individual pyramidal cells in the basolateral amygdala. *Brain Res.* **1035**, 32–40 (2005).